Proton NMR Investigation of Substrate-Bound Heme Oxygenase: Evidence for Electronic and Steric Contributions to Stereoselective Heme Cleavage†

Griselda Hernández,‡ Angela Wilks,§ Roberto Paolesse,‡ Kevin M. Smith,‡ Paul R. Ortiz de Montellano,§ and Gerd N. La Mar*,‡

Department of Chemistry, University of California, Davis, California 95616, and Department of Pharmaceutical Chemistry, University of California, San Francisco, California 94143

Received January 11, 1994; Revised Manuscript Received March 25, 1994®

ABSTRACT: The substrate-bound form of the enzyme heme oxygenase (HO), which catalyzes the stereospecific α-meso bridge cleavage of hemin to yield biliverdin IXα, has been investigated by ^{1}H NMR in both its primarily high-spin and its cyanide-inhibited low-spin forms. Both derivatives yield ^{1}H NMR spectra indicative of extensive heterogeneity that is largely resolved when a 2-fold-symmetric hemin substrate is bound. The structural origin of the heterogeneity is shown to result from ~1:1 isomeric binding of the native hemin substrate in the binding pocket. The substrate orientational disorder is about the α,γ-meso axis, as established on the basis of 2D NMR experiments that identify characteristic aromatic van der Waals contact in the substrate binding pocket. The isomeric substrate–HO complexes exhibit differential cyanide affinity, and the ratio of isomers is sensitive to the hemin 2,4-substituents. The assignment of hemin signals by isotopic labeling and 2D NMR methods reveals a contact shift pattern that reflects an unusual hemin electronic structure that is characterized by large differences in delocalized spin density for the two positions within a given pyrrole, rather than the more conventional large differences between adjacent pyrroles. This pattern of spin density delocalized primarily to the pyrrole positions adjacent to the α,γ-meso axis can be rationalized by postulating a direct electronic perturbation of the hemin by the protein matrix in the form of an anionic side chain close to the α-meso carbon. Similar influences on hemin electronic structure, in the form of chemical substitution of the meso positions, have been observed in iron porphyrin compounds and successfully modeled by simple molecular orbital theory (Tan *et al.*, 1994). This is interpreted as evidence for a direct electronic effect by HO to activate the α-meso position for electrophilic rather than nucleophilic attack. The unique contact shift pattern is present to different degrees for the two hemin orientations, is strongly pH dependent, and is largely abolished at acidic pH. Portions of several heme pocket residues are located, and it is shown that the pattern of the dipolar shifts for these residues, which likely reflects the distal steric influence on the tilt of the coordinated cyanide, differs significantly for the two substrate orientations. The variable electronic and steric influences of the protein matrix on the two hemin substrate orientations suggest heterogeneous, pH-dependent kinetics, but unaltered stereoselectivity in the enzyme reaction, and may account for the wide range of activity of HO with respect to a variety of peripherally modified hemins.

Heme oxygenase (HO[1]) catalyzes the NADPH cytochrome P-450 reductase-dependent oxidation of heme to biliverdin (Tenhunen et al., 1969). Heme oxygenase is thus responsible for the catabolism of heme. The degradation of heme may be important for more than the regulation of heme levels, because recent work suggests that the carbon monoxide generated by heme oxygenase in the brain may play a role as a neural messenger (Verma et al., 1993; Zhuo et al., 1993; Stevens & Wang, 1993). Heme oxygenase is a membrane-bound protein that has been purified from several sources, including rat liver (Yoshida & Kikuchi, 1979), pig spleen (Yoshida & Kikuchi, 1978), bovine spleen (Yoshinaga et al., 1982), and chicken liver (Bonkovsky et al., 1990). Two isozymes, HO-1 and HO-2, have been identified (Shibahara et al., 1985; Yoshida et al., 1988; Evans et al., 1991; Maines et al., 1986; Maines, 1992). The isozymes from various species show only 50% identity in amino acid sequence, but all share a number of common features (McCoubrey & Maines, 1993). Among these is a conserved 24 amino acid domain that includes an essential histidine residue (McCoubrey & Maines, 1993; Ishikawa et al., 1992). The carboxyl-terminal portion of the enzyme shows a low frequency of amino acid conservation but a high degree of conservation in its hydropathic profile, indicating the importance of the membrane-spanning region that is inserted into the endoplasmic reticulum (McCoubrey & Maines, 1993; Wilks & Ortiz de Montellano, 1993). We have recently developed a high-yield heterologous expression system that produces a soluble, fully active, HO-1 enzyme in which the last 23 carboxy-terminus amino acids have been deleted (Wilks & Ortiz de Montellano, 1993).

The strong similarity of the optical spectrum of the CO-bound substrate complex of HO to that of the same myoglobin complex had led to the proposal of an axially coordinated His (Yoshida & Kikuchi, 1978, 1979). More recent resonance Raman and ESR studies provide evidence for a neutral axial

† This research was supported by grants from the National Institutes of Health (HL 16087, HL 22252, DK 30297, and DK26743). R.P. acknowledges the support of a CNR fellowship.

* Address correspondence to this author.

‡ University of California at Davis.

§ University of California at San Francisco.

® Abstract published in *Advance ACS Abstracts,* May 1, 1994.

[1] Abbreviations: HO, heme oxygenase; PHIX, protohemin IX; PHIII, protohemin III; DHIX, deuterohemin IX; DHIII, deuterohemin III; NMR, nuclear magnetic resonance; ppm, parts per million; 2D, two-dimensional; NOE, nuclear Overhauser effect; DSS, 2,2-dimethyl-2-silapentane-5-sulfonate; COSY, 2D correlation spectroscopy; NOESY, 2D nuclear Overhauser spectroscopy; Mb, myoglobin; Hb, hemoglobin.

0006-2960/94/0433-6631$04.50/0

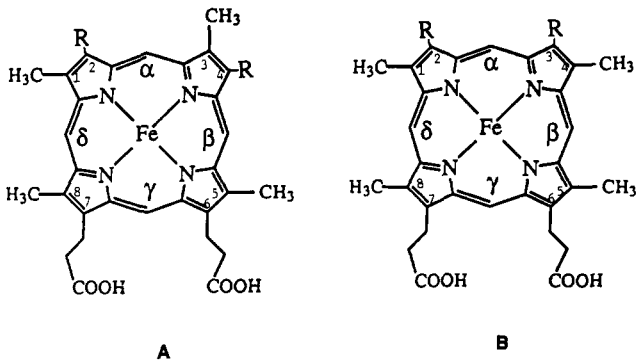

FIGURE 1: Structure of the type IX isomers (A) and the type III isomer (B) of protohemin (R = vinyl) and deuterohemin (R = H).

His that is unlikely to donate electron density to the iron to facilitate dioxygen bond cleavage and suggest that the O_2 activation process may be modulated by distal residues (Sun et al., 1994; Takashi et al., 1994). Although some important intermediates in HO catalysis have been identified (Beale, 1993; Maines, 1992), key issues such as how the enzymes bind hemin and activate O_2 have yet to be resolved. Nuclear magnetic resonance is capable of providing very detailed information on the molecular structure of enzymes in solution, but for large enzymes such as HO, spectral congestion becomes a serious problem. This problem is obviated somewhat in paramagnetic proteins in which the hyperfine interaction not only provides resolution for many of the active-site resonances but the pattern of hyperfine shifts also provides valuable information on the electronic structure and magnetic properties of the bound substrate and, through the magnetic properties of the heme iron, steric influences on ligand binding (Satterlee, 1985).

We report herein on a 1D and 2D proton NMR investigation of the high-spin, substrate-bound complex of heme oxygenase and its low-spin, cyanide-inhibited derivative. The latter complex, like metcyanomyoglobins, ferricytochromes *b* and *c*, and cyanide-inhibited heme peroxidases, can be expected to exhibit well-resolved ^{1}H NMR spectra suitable for study by modern 2D NMR methods (La Mar & de Ropp, 1993). We consider two substrates for comparison purposes: the natural protohemin IX (PHIX) (R_2 = R_4 = vinyl in Figure 1A) and the synthetic deuterohemin IX (DHIX) (R_2 = R_4 = H in Figure 1A). These two substrates exhibit significantly different activity with HO (Frydman & Frydman, 1987) and introduce the heme peripheral substituents, a hydrogen and a methyl, which allow elucidation of the heme electronic structure (Walker & Simonis, 1993). Both PHIX and DHIX possess only pseudo-2-fold symmetry about the α,γ-meso axes, as shown in Figure 1A. Hence, we include in our study two additional substrates that possess true 2-fold symmetry about the α,γ-meso axes: protohemin III (PHIII) (R_2 = R_3 = vinyl in Figure 1B) and deuterohemin III (DHIII) (R_2 = R_3 = H in Figure 1B).

MATERIALS AND METHODS

Sample Preparation. Heme oxygenase was expressed, purified, and reconstituted with the various hemins, as described previously (Wilks & Ortiz de Montellano, 1993). Samples were exchanged into ^2H_2O 50 mM in phosphate on Centricon 10 filtration units and an Amicon ultrafiltration cell to give a final protein concentration of 0.2–1.8 mM. Protohemin III was synthesized as reported previously (Smith et al., 1986a) and was converted to deuterohemin III by the resorcinol melt method (Fuhrhop & Smith, 1975). The deuterium-labeled hemins used were protohemin IX, [5-$^2H_3$]protohemin IX, [1,3-$^2H_6$]protohemin IX, [1-$^2H_3$]protohemin IX, [3-$^2H_3$]protohemin IX, and [2,4-(β-$^2H)_2$]protohemin IX, and the unlabeled hemins were protohemin III, deuterohemin IX, and deuterohemin III. Their syntheses have been reported previously (Smith et al., 1983, 1986b, 1988). A solution of potassium cyanide prepared in the same solvent was added to generate the cyano complex. pH titration of protohemin IX-heme oxygenase (PHIX-HO) was performed over the pH range 4.9–9.0 by dropwise addition of diluted NaO^2H or ^2HCl in ^2H_2O. The pH effect was found to be reversible by back-titration. pH titration of deuterohemin IX-heme oxygenase was performed over the pH range 6.6-9.0. The pH value was not corrected for the isotope effect. To observe exchangeable protons, protohemin IX–heme oxygenase cyano complex was prepared in 0.1 M phosphate buffer in 90% H_2O/10% D_2O.

NMR Data. The 300-MHz ^{1}H NMR spectra of the high-spin complexes were obtained on a General Electric NMR Ω-300 spectrometer. Typical high-spin spectra were collected with 2048 complex points over a 60-kHz spectral width, with a pulse repetition rate of 10–20 s^{-1}. The 500-MHz ^{1}H NMR spectra of low-spin cyano complexes were obtained in a General Electric NMR Ω-500 spectrometer. Typical data were collected with 8192 points over a 31-kHz spectral width with a pulse repetition rate of 2.5 s^{-1}. The residual solvent lines for both 300- and 500-MHz spectra were suppressed with a low-power presaturation pulse. To observe fast-relaxing protons, a pulse repetition rate of 14.5 s^{-1} was acquired. High-spin/low-spin mixture spectra were collected at 300 MHz using the parameters to optimize either the low-spin or high-spin spectrum.

Steady-state nuclear Overhauser effect (NOE) spectra were performed using a low-power decoupler pulse to saturate the resonance of interest for ~100 ms, as previously described in detail (Thanabal et al., 1987). Data acquired with the decoupler on-resonance were interleaved with those acquired with the decoupler off-resonance. Nonselective T_1 data were obtained by the basic 180–τ–90° pulse sequence using 8192 points over a 21052-Hz bandwidth. For the 500-MHz ^{1}H NMR spectra of PHIX-HO-CN in 90:10 $^1H_2O/^2H_2O$, data were collected in the 5–25 °C range using a soft pulse sequence (Hore, 1983) with the carrier at 35 ppm, with and without saturating the solvent signal. NOESY data were acquired in ^2H_2O at 20 and 25 °C using a standard phase-sensitive (TPPI) pulse sequence (Marion & Wüthrich, 1983) on a 400-MHz Bruker AMX spectrometer (17 241 Hz spectral width, 512 blocks of 1024 points) and a 500-MHz General Electric Ω-500 spectrometer (21 052 Hz spectral width, 512 blocks of 1024 points with 640–960 scans per block); the mixing times used were 10, 20, and 40 ms. *n*-type (MCOSY) data (Bax, 1982) were collected at 20 °C on the General Electric NMR Ω-500 spectrometer with 256 blocks of 1024 complex points over a sweep width of 21 052 Hz; each block consisted of 960 scans. All 2D data sets were acquired with solvent suppression achieved by direct saturation in the relaxation rate period and a repetition rate of 3 s^{-1}.

1D spectral data were treated with exponential apodization to increase signal to noise; 5-Hz line broadening was employed for low-spin complex spectra, and 20–50 Hz was used for high-spin complexes and/or to emphasize fast-relaxing proton resonances from low-spin complexes. NOESY data sets acquired on the Bruker AMX-400 were transferred to a Silicon Graphics IRIS and processed using the Hare Research software package FELIX (version 1.1), using 40-deg-shifted sine-bell-squared apodization applied over 512 points and zero-

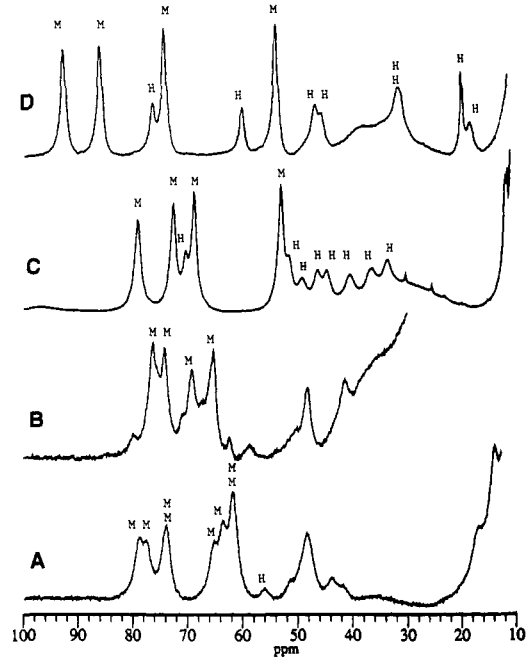

FIGURE 2: 300-MHz ^{1}H NMR spectra of (A) 1.8 mM PPIX-HO in ^2H_2O (pH 7.2) at 20 °C and of (B) 0.8 mM DHIX-HO in ^2H_2O (pH 7.2) and 20 °C. The 300-MHz ^{1}H NMR spectra of (C) 2.0 mM resting-state horseradish peroxidase in ^2H_2O (pH 7.0) at 35 °C and (D) 2.0 mM sperm whale cyanometmyoglobin in ^2H_2O (pH 7.5) at 25 °C are reproduced for comparison. Peaks are labeled M (vinyls) and H (single protons).

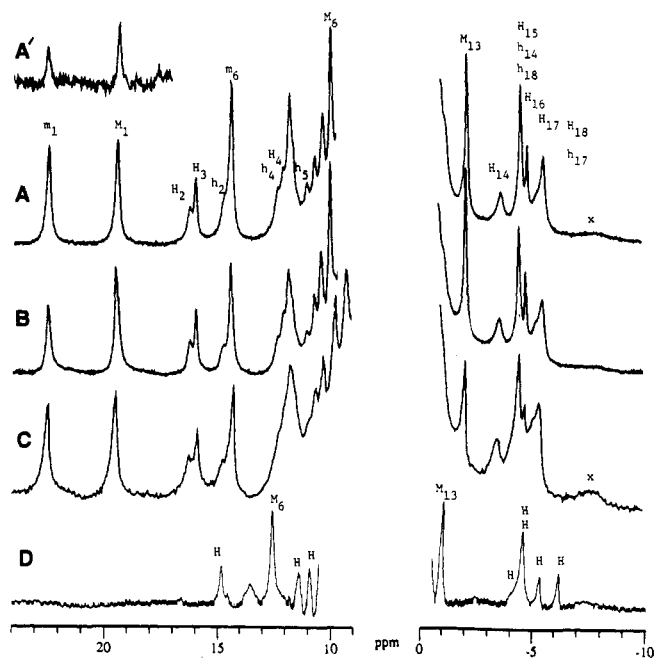

FIGURE 3: Resolved portions of the 500-MHz ^{1}H NMR spectra in ^2H_2O (pH 7.4) at 25 °C: (A) immediately after the addition of excess KCN to 1.8 M PPIX-HO to form the PPIX-HO-CN complex (peaks are labeled M_i,H_i for methyls and single protons from isomer X and m_i,h_i for methyls and single protons of isomer Y, the inset in A' shows the methyl peaks m_i and M_i when only 0.1 molar equiv of cyanide is added, and the unequal intensities show that m_i and M_i arise from different molecular forms with different cyanide affinities); (B) the same sample as in A, one week after the addition of KCN when the X,Y isomer distribution has reached equilibrium (the spectrum is scaled vertically so as to keep M_i the same height as in trace A and shows that H_2, H_3, M_6, M_{13}, and H_4 scale similarly with M_1 and hence arise from isomer X, while h_2, m_6, and h_{18} are reduced relative to trace A and hence arise from isomer Y); (C) same trace as in A but collected with a pulse repetition rate (14.5 s^{-1}) that emphasizes the rapidly relaxed proton under the composite at ca. −5 ppm and the very broad peak labeled x; (D) 500-MHz ^{1}H NMR trace of 0.3 mM PHIII-HO-CN in ^2H_2O (pH 7.6) at 20 °C (methyl and single-proton peaks are labeled M_i and H_i, respectively). Note the absence of methyl peaks in the 20–25 ppm window and the sharply reduced number of resonances; the upfield peak at −2 ppm appears as a composite of several single-proton peaks.

filled to 1024 points in both dimensions. The t_2 data were phase-corrected and base-line-straightened. NOESY data sets acquired in the General Electric Ω spectrometer were processed on a SUN 3/260 workstation. The 30- and 40-deg-shifted sine-bell-squared apodizations were applied over 1024 and 256 points on t_2 and t_1, respectively. The t_2 data were phase-corrected and base-line-straightened. All data sets were zero-filled to 1024 × 1024 points prior to Fourier transformation. MCOSY data sets were processed on a SUN 3/260 workstation using an unshifted sine-bell-squared window function over the collected data in both dimensions.

RESULTS

Molecular Heterogeneity

Resting-State HO. The 300-MHz ^{1}H NMR spectrum of 1.6 mM PHIX-HO in ^2H_2O (pH 7.2) at 20 °C is shown in Figure 2A and is compared to that of resting-state horseradish peroxidase in Figure 2C and that of sperm whale aquometmyoglobin in Figure 2D. In contrast to the latter two proteins, which exhibit one set of four heme methyls and seven single proton signals in the resolved low-field spectral window indicative of a single dominant molecular species in solution, PHIX-HO displays evidence for extensive heterogeneity. Thus, if the resolved peak at 56 ppm arises from a single proton, then the peaks in the 60–90 ppm window reflect intensity closer to that of eight than that of four methyl groups. The similar intensities of the two lowest field peaks at 77.5 and 79.1 ppm, each of which is approximately 3 times that of the 56 ppm peak, suggest comparable populations of at least two species. The 300-MHz ^{1}H NMR trace of 0.8 mM DHIX-HO in ^2H_2O (pH 7.2) at 20 °C is illustrated in Figure 2B. The two lowest field peaks at 76.2 and 80.3 ppm, which are most likely heme methyls in any high-spin ferric hemoprotein, exhibit unequal intensity, again indicating molecular heterogeneity but with very unequal populations of the two species. Unfortunately, the ^{1}H NMR spectra of these largely high-spin species in Figure 2A,B do not afford the resolution necessary to quantitate the heterogeneity or identify its molecular origin.

Cyanide-Inhibited PHIX-HO. The resolved portions of the 500-MHz ^{1}H NMR spectrum of PHIX-HO-CN in the presence of excess CN^- in ^2H_2O (pH 7.4) at 20 °C immediately after the addition of CN^- are given in Figure 3A. The range of hyperfine-shifted resonances, their line widths (90–150 Hz), and the T_1 values (30–200 ms) for the majority of the resolved peaks (Table 1) are typical of low-spin ferric hemoproteins (Satterlee, 1986), although the number of resonances outside the 0–10 ppm diamagnetic envelope is unusually large. Variations in temperature (not shown) and pH (Figure 4 and supplementary material) reveal only five signals that retain essentially identical three-proton intensity under all conditions (labeled m_1, m_6, M_1, M_6, and M_{13} in Figure 3A) relative to obvious one-proton signals (labeled H_2, H_3, and H_{14} in Figure 3A). All other peaks outside the 0–10 ppm envelope are composites of several peaks each with single proton intensity. In spite of the fact that apparent methyl peaks m_1 and M_1 have identical intensities in Figure 3A, it is clear that they arise from two different molecular species. Thus, when only a 0.1 molar equiv of CN^- is added to PHIX-HO, the intensities

Table 1: ^{1}H NMR Spectral Parameters for the Cyanide Complex of Isomeric Bound Protoheme IX to Heme Oxygenase[a]

	isomer X[b]			isomer Y[c]		
i (for χ_i)	assignment	shift (ppm)	T_1 (ms)	assignment	shift (ppm)	T_1 (ms)
1	3-CH_3	22.5	130	3-CH_3	19.1	120
2	axial His $C_\beta H$ (?)	16.0	120	axial His $C_\beta H$ (?)	14.4	~100
3	2-H_α	16.0	130	*d*		
4	6-H_α	11.9	*e*	7-H_α	12.2	*e*
5	6-H_α	11.4	*e*	7-H_α'	10.8	*e*
6	5-CH_3	10.0	*e*	8-CH_3	14.4	120
7	aromatic	6.78	*e*	aromatic	6.75	*e*
8	aromatic	6.40	*e*	aromatic	6.35	*e*
9	axial His $C_\beta H'$ (?)	3.8	*e*	axial His $C_\beta H'$ (?)	5.18	*e*
11	CH of R	2.45	3	*d*		
12	?	0.40	*e*	*d*		
13	CH_3 of R	−2.3	170	*d*	0	
14	CH_2 of Q	−3.7	85	CH_2 of Q′	−4.8	*e*
15	2-$H_{\beta t}$	−4.8	*e*	*d*		
16	2-$H_{\beta c}$	−5.1	*e*	*d*		
17	CH_2 of Q	−5.4	~35′	CH_2 of Q′	−5.86	
18	α-meso-H	−5.8	~40′	α-meso-H	−4.8	

[a] Data were obtained in ^2H_2O (pH 7.1) at 20 °C, with shifts referenced to DSS. [b] Isomer X with peak $\chi_i = M_i,H_i$ in Figures 3A, 7, and 8. [c] Isomer Y with peak $\chi_i = m_i,h_i$ in Figures 3A, 7, and 8. [d] Comparable peaks not resolved outside the 0–10 ppm window for isomer Y. [e] Not sufficiently resolved to allow an estimate of T_1. [f] From null point, τ_{null}, $T_1 = \tau_{null}/\ln 2$.

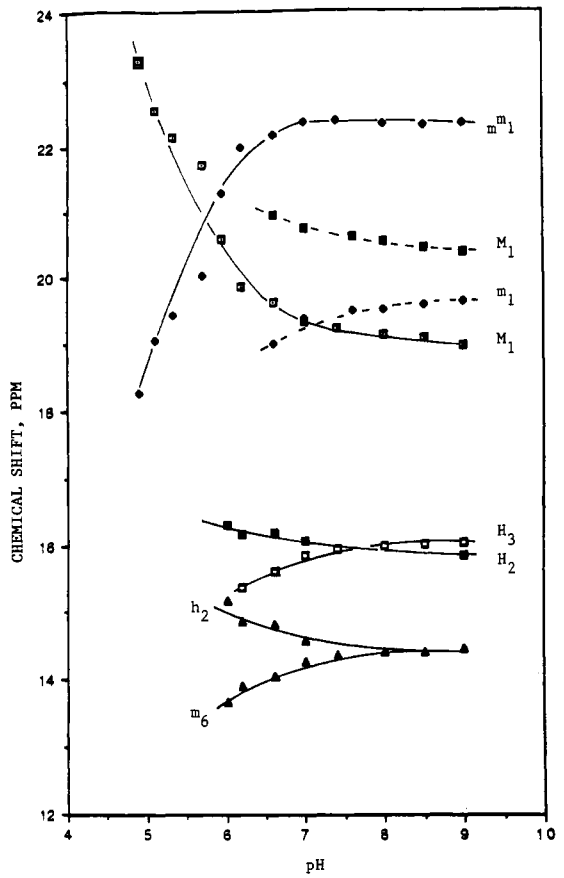

FIGURE 4: Plot of the chemical shift for the resolved low-field resonances of PHIX-HO-CN (solid lines) and DHIX-HO-CN (dashed lines) in ^2H_2O, at 20 °C, as a function of solution pH. The resonances are labeled as in Figures 3 and 5. The lines are not fits to a p*K*, but are shown only to reflect the continuity of the data. While the pH profile was completely reversible, pH instabilities at acidic pH resulted in significant uncertainties in pH values.

of the PHIX-HO-CN methyl signals m_1 and M_1 differ by a factor of 1.4, as shown in inset A′ to Figure 3A, indicating that the peaks arise from two molecular forms of PHIX-HO that differ in cyanide affinity. Since excess CN^- yields equal intensities for m_1 and M_1, the species giving rise to peak M_1 exhibits ~40% greater cyanide affinity than the species responsible for peak m_1.

The 1:1 heterogeneity in initially ligated PHIX-HO-CN is confirmed by the time dependence of its ^{1}H NMR spectrum. Thus, over a period of several days, the ^{1}H NMR spectrum in Figure 3A changes, with one set of resonances increasing while the other set decreases in intensity, until an equilibrium is reached where the relative amounts of the two species, given by methyl peak intensities m_1:M_1, are ~2:3, as shown in Figure 3B. We define the major component at equilibrium as species X, with resonances labeled M_i and H_i for methyl groups and single-proton peaks, respectively; the minor component is defined as species Y, with resonances labeled m_i and h_i for methyl groups and single-proton peaks, respectively. Comparison of the relative intensities in Figure 3A,B clearly identifies peaks M_1, M_6, M_{13}, H_2, H_3, and H_{14} as arising from isomer X and peaks m_1, m_6, h_2, and likely h_{18} as arising from isomer Y. All other peaks are complicated composites for which a simple comparison of the relative intensities in Figures 3A,B is insufficient to identify their isomer origin. One partially resolved broad (600 Hz) and strongly relaxed (T_1 ~ 3 ms) upfield peak x at −9.7 ppm is optimally collected with a rapid (14.5 s^{-1}) pulse repetition rate, as shown in Figure 3C.

The pH influence on the well-resolved low-field signals is illustrated in Figure 4. The shifts appear to approach pH independence in the pH range 8–9, but exhibit strong pH dependence at acidic pH, indicative of a p$K < 6$. The pH changes were found to be reversible, although the substrate-bound complex was found to precipitate extensively at low pH. We note that isomers X and Y are differentiated by their pH behavior, in that the lowest field methyl peaks are strongly shifted to low-field (M_1) and high-field (m_1), respectively, at acidic pH.

Cyanide-Inhibited DHIX-HO. The resolved portions of the 500-MHz ^{1}H NMR spectrum of DHIX-HO immediately after the addition of excess CN^- in ^2H_2O (pH 6.6) at 20 °C are shown in Figure 5A, and the same region after 18 h under the same conditions is illustrated in Figure 5B. The initial spectrum is consistent with two sets of peaks: low-field methyl peaks M_i and upfield single-proton peaks H_i for a major isomer X′ and similar low-field methyl peaks m_i (see below) with upfield single-proton peaks h_i for minor isomer Y′. The ratio of M_1:m_1 is initially ~4:1 (Figure 5A) and reaches 3:2 at equilibrium (Figure 5B). Hence, DHIX-HO is also heterogeneous with two isomers present. Raising the pH moves peaks M_1 and m_1 closer together while leaving the positions of the upfield peaks essentially unchanged, as shown in Figure 5B,C. The two methyl peaks move in the opposite direction with pH, as shown in Figure 4.

Symmetric Substrates. The binding of substrates that possess 2-fold symmetry, PHIII and DHIII, to HO in the presence of excess cyanide yields the 500-MHz ^{1}H NMR spectrum of PHIII-HO-CN (Figure 3D) and that of DHIII-HO-CN (Figure 5D). In each case, inspection of the spectrum reveals that the number of resolved resonances is sharply reduced relative to the analogous type IX substrates, and the relative intensities of the peaks, which are independent of time, are indicative of a single dominant molecular species in each case. This is particularly noteworthy for DHIII-HO-CN, where the narrow single-proton peaks upfield of ca. −10 ppm must originate from the pyrrole-H's at positions 2 and 3. For DHIX-HO-CN (Figure 5A–C), four such peaks, H_{11},

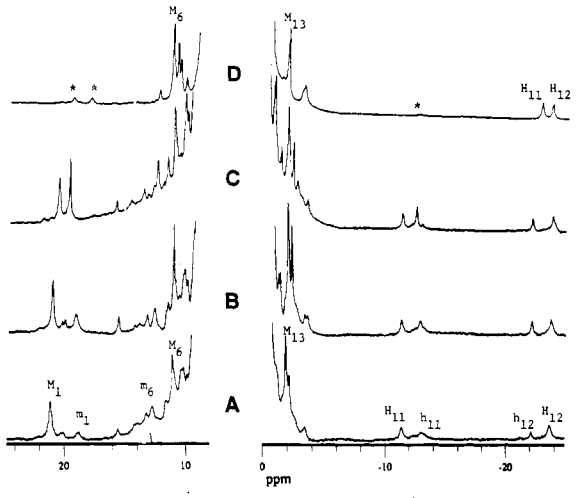

FIGURE 5: Resolved portions of the 500-MHz ^{1}H NMR spectra (A) ~1 h after the addition of excess cyanide to DHIX-HO in ^2H_2O (pH 6.6) at 20 °C; (B) same sample as in trace A with the same solution conditions after 2 days (note the increase in intensity of Y isomer peaks m_i,h_i (methyl, single protons) at the expense of isomer X peaks M_i,H_i (methyls, single protons); (C) trace in D_2O (pH 8.0) at 20 °C, which shows shift changes for M_1,m_1 and line narrowing for m_i; (D) trace in ^2H_2O (pH 8.6) at 20 °C of DHIII-HO-CN with peaks labeled M_i (methyls) and H_i (single protons). Note the reduced number of resolved peaks in D relative to those in traces A–C. The peaks labeled with an asterisk are identified as arising from a small amount of free dicyanodeuterohemin complex in solution.

H_{12}, h_{11}, and h_{12}, are observed, while only two such peaks, H_{11}, and H_{12}, are seen in DHIII-HO-CN (Figure 5D). Thus, the molecular heterogeneity in the substrate complexes of PHIX and DHIX appears to reflect the absence of the 2-fold symmetry axis about the α,γ-meso axis, with the two species likely resulting from the isomeric incorporation of the heme in the substrate binding site. This hypothesis is confirmed by the assignments below.

Resonance Assignments

Isotopic Labeling of the Heme. The severe spectral congestion even in the region outside 0–10 ppm due to the presence of two isomers, together with the weak cross peaks in 2D NMR maps (see below), dictates the use of specifically deuterated PHIX substrate to provide the initial unambiguous assignment necessary to establish heme orientational disorder and elucidate the hemin electronic structure. The isomer origin of the methyl peaks, M_1, M_6, and M_{13} from isomer X and m_1 and m_6 from isomer Y, has been determined from a comparison of Figure 3A,B. The resolved portions of the 500-MHz ^{1}H NMR spectra of the cyano complexes of HO bound by three selectively deuterated PHIX substrates are illustrated in Figure 6B–D, where they are compared to that of native PHIX-HO-CN in Figure 6A. Deuteration of both the 1- and 3-methyl groups (Figure 6B) and only the 3-methyl group (Figure 6C) abolishes only the two low-field methyl peaks m_1 and M_1 among signals outside 0–10 ppm, dictating that both m_1 and M_1 arise from 3-CH_3. Deuteration of solely the 5-methyl group leads to intensity loss solely for M_6 (Figure 6D), identifying it as the 5-CH_3 of isomer X. Methyl peak M_{13} cannot arise from the heme since it exhibits spin coupling to another proton (Figure 7C). On the other hand, the absence of spin coupling to m_6 argues that it arises from the sole

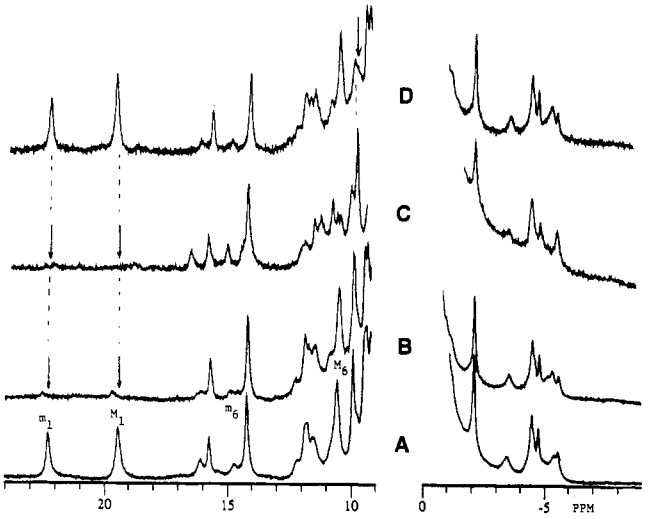

FIGURE 6: Resolved portions of the 500-MHz ^{1}H NMR spectra of the cyano complex of HO bound by protohemin substrate, which is selectively deuterated at the (B) 1- and 3-methyl positions; (C) 3-methyl position; and (D) 5-methyl position. Peak intensity loss due to deuteration is indicated by vertical arrows; the reference trace for the unlabeled PHIX substrate complex is shown in A.

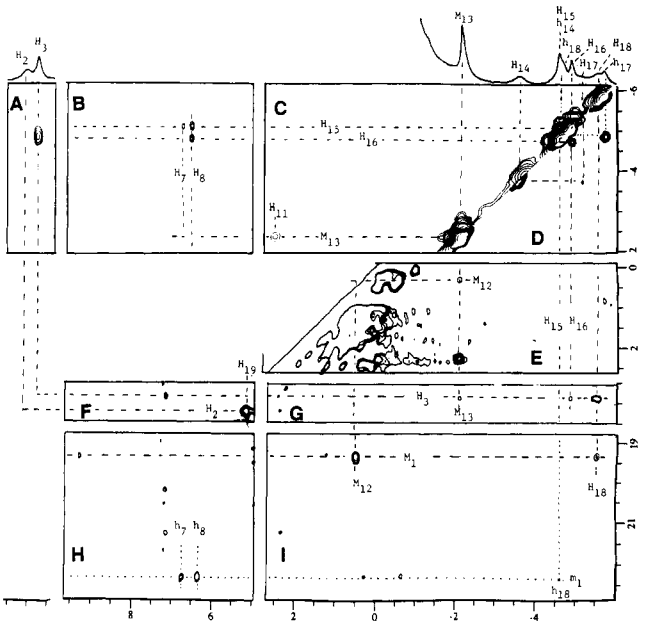

FIGURE 7: Portions of the 500-MHz MCOSY (A and C) and 20-ms mixing time NOESY (B, D–I) of PHIX-HO-CN in ^2H_2O (pH 7.1) at 20 °C, illustrating cross peaks that identify the isomer origin and functionality of the upfield hyperfine-shifted resonances and the dipolar contacts with aromatic residues of heme substituents. The resolved peaks are labeled above panels A and C. The MCOSY cross peak between H_3 and H_{15},H_{16} splits into two peaks at higher resolution.

unlabeled heme methyl, i.e., the 8-CH_3 of isomer Y.[2] The deuteration of the H_β's of both vinyl groups (not shown) leads to some apparent intensity loss only in the multiproton composite centered at –4 ppm, indicating the presence of one or two vinyl H_β signals in this window (see below); the farthest upfield peak, h_{18}, does not reflect an intensity loss. Further signal identification requires the use of 2D NMR methods.

2D NMR Methods. The samples of PHIX-HO-CN presently available (~1.8 mM) afforded 2D NMR spectra

[2] The signals from 1-CH_3 and 8-CH_3 for isomer X, as well as from 1-CH_3 and 5-CH_3 for isomer Y, must resonate under the diamagnetic envelope 0–10 ppm.

with relatively few and weak cross peaks when compared to other low-spin ferric proteins, such as either cyanometmyoglobin (Emerson & La Mar, 1990a) or cyanide-inhibited heme peroxidases (de Ropp et al., 1991). In part, this must be due to the limited sample concentration and the presence of two isomers, but it may also reflect a more open heme crevice. Moreover, all samples exhibited limited stability with respect to spontaneous cyanide release and pH changes that altered chemical shifts. Hence, we restrict our use of 2D NMR to addressing the strongly hyperfine-shifted heme signals and to identifying the isomer origin of the strongly hyperfine-shifted amino acid resonances, particularly those in the spectral window upfield of −2 ppm. This latter goal is achieved by observing NOESY cross peaks to the target upfield peaks from those resonances whose isomer origin could be unambiguously determined from the intensity pattern in Figure 3A,B, i.e., M_1, H_2, H_3, M_6, M_{13}, and H_{14} from isomer X and m_1, h_2, m_6, and likely h_{18} from isomer Y.

Figure 7 exhibits portions of the MCOSY (Figure 7A,C) and 20-ms mixing time NOESY maps[3] (Figure 7B,D–I) that display the dipolar contacts of the two low-field 3-CH_3 peaks, m_1, and M_1, and identify the isomer origin of the upfield resonances. The only MCOSY cross peaks involving resolved resonances outside the 0–14 ppm window are between methyl peak M_{13} and peak H_{11} (Figure 7C) and between the low-field peak H_3 and each of the upfield peaks, H_{15} and H_{16} (Figure 7A). The latter scalar connectivity pattern, together with their NOESY cross peaks in Figure 7G, uniquely identifies H_3, H_{15}, and H_{16} as the H_α, $H_{\beta c}$, and $H_{\beta t}$ of a vinyl group from isomer X. Moreover, the absence of a detectable NOESY cross peak from either the $H_\alpha(H_3)$ or H_β's(H_{15},H_{16}) to the X isomer 3-CH_3 (M_1) demands that H_3, H_{15}, and H_{16} arise from the 2-vinyl rather than the 4-vinyl group. The X isomer 4-vinyl and both Y isomer vinyl groups must resonate in the crowded 0–10 ppm window.

Inspection of the NOESY maps reveals relatively few cross peaks in the 0–10 ppm window for the low-field 3-CH_3 peaks m_1 and M_1, with the two 3-CH_3 peaks exhibiting very different patterns that are indicative of different protein environments (Figure 7H,I). In particular, the X isomer 3-CH_3 peak M_1 fails to exhibit any cross peaks to the aromatic window 6–8 ppm, while the Y isomer 3-CH_3 peak m_1 exhibits strong cross peaks to two peaks, h_7 and h_8, in that spectral window, with essentially temperature-independent shifts that dictate that they arise from an aromatic side chain (Thanabal et al., 1987). Hence, the 3-CH_3 in isomer Y, but not in isomer X, must be in van der Waals contact with an aromatic amino acid. It is noted, however, that the 2-vinyl group 2H$_\beta$'s (H_{15} and H_{16}) of isomer X each exhibit strong cross peaks to two peaks, H_7 and H_8, with temperature-insensitive chemical shifts in the 6–8 ppm window (Figure 7B), dictating that the 2-vinyl group of isomer X has van der Waals contact with an aromatic amino acid. Two broad upfield signals, H_{18} and h_{18}, each fail to exhibit COSY cross peaks, but yield moderately strong resonance NOESY cross peaks to M_1 and m_1, respectively, the 3-CH_3 peaks of isomers X and Y, respectively (Figure 7I). The signal H_{18}, moreover, exhibits a NOESY cross peak to the identified 2-vinyl H_α of the X isomer (Figure 7G). The line width (~150 Hz, as determined in a steady-state NOE difference spectrum; not shown) and apparent short T_1 (~25 ms) of peak H_{18} support the assignment to the α-meso-H of isomer X. The similar line width of h_{18} suggests that it arises from the α-meso-H of isomer Y.

[3] The 20-ms mixing time was found to be optimal for sensitivity, as was also the case for horseradish peroxidase (Sette et al., 1993).

The isomer X methyl peak, M_{13}, exhibits a COSY (Figure 7C) and a NOESY cross peak to H_{11} (Figure 7E), which identifies a non-coordinated amino acid CH_3CH fragment. No additional protons arising from this residue could be identified by COSY. The methyl peak M_{13} for isomer X, however, exhibits a strong NOESY cross peak to 2-vinyl H_α-(H_3), as shown in Figure 7G, as well as steady-state NOEs to α-meso-H (H_{18}) and 3-CH_3 (M_1) (not shown). Thus, the non-coordinated amino acid side chain is close in contact with the heme near the junction of pyrroles A and B (Figure 1A). The non-resolved likely methyl peak M_{12} exhibits a weak NOESY cross peak to M_{13} (Figure 7E) and a very strong cross peak to M_1 (3-CH_3) (Figure 7I). The identity of M_{12} is obscure, but the failure to detect COSY cross peaks common to M_{13} and M_{12} makes it likely that they arise from different residues. Lastly, the methyl peak M_{13} also exhibits a strong NOESY peak to one of the two aromatic protons, H_8, which also displays NOESY cross peaks to 3-CH_3 peak M_1 (Figure 7B). Hence, both the aromatic side chain responsible for signals H_7 and H_8 and the aliphatic side chain with methyl M_{13} are on the same side of the heme.

Two protons, H_{14} (T_1 ~ 80 ms) and H_{17} (T_1 ~ 30 ms), each exhibit NOESY cross peaks to each other but to nothing else in the upfield window (Figure 7D). Saturation of H_{14} results in an approximately −30% steady-state NOE to H_{17} (not shown), indicating that H_{14} and H_{17} are methylene protons for isomer X (Thanabal et al., 1987). The isomer Y peaks h_{14} and h_{17} exhibit similar properties. The only NOESY cross peaks from either the H_{14},H_{17} or h_{14},h_{17} pairs are to un-resolved and unassigned peaks in the window 12–14 ppm (not shown). It is noted that the Y isomer peaks h_{14} and h_{17} cannot arise from a vinyl group and more likely represent the analogs of the X isomer peaks H_{14} and H_{17}. Moreover, the significant relaxation (line width ~100–150 Hz, T_1 ~ 30–80 ms) indicates that the H_{14} and H_{17} do not arise from the propionate H_α's or H_β's, which relax at rates generally comparable to, or slower than, those of heme methyls. Hence, we conclude that H_{14} and H_{17} (and likely h_{14} and h_{17}) arise from a non-coordinated residue in isomers X and Y, respectively, that is not in contact with pyrrole A or B and likely not in contact with pyrrole D of isomer X or pyrrole C of isomer Y (see below). It is important to note that no signals are observed for the Y isomer that are analogous to the X isomer fragment $CH_3(M_{13})CH(H_{11})$ in the upfield resolved window. Any such fragment for the Y isomer must have a methyl shift at least 3 ppm to lower field than M_{13} and, hence, falls under the intense diamagnetic envelope.

The broad (600 Hz) and strongly relaxed (T_1 ~ 3 ms) upfield peak x has its intensity insufficiently defined to allow unambiguous assignment to one or the other isomer, but it appears to correlate better with isomer X. However, the short T_1, when compared to that of the heme methyl (~120 ms), dictates[4] a distance from the iron of ~3.5 Å, which is consistent with a peak arising from one of the coordinated His imidazole nonlabile protons. Similarly relaxed and shifted signals that could be assigned to axial His CH's are observed in low-spin ferric myoglobins (Emerson & La Mar, 1990a) and peroxidases (Thanabal et al., 1987).

Identification of resonances in the low-field envelope in the window 10–12 ppm met with more limited success; relevant NOESY cross peaks are shown in Figure 8. Strong NOESY cross peaks within the pairs of protons H_4,H_5 and h_4,h_5 identify

[4] The relaxation is assumed to be primarily dipolar, with $T_i^{-1} \propto R_i^{-6}$, where R is the distance to the iron; a heme methyl has R ~ 6.1 Å (Cutnell et al., 1981).

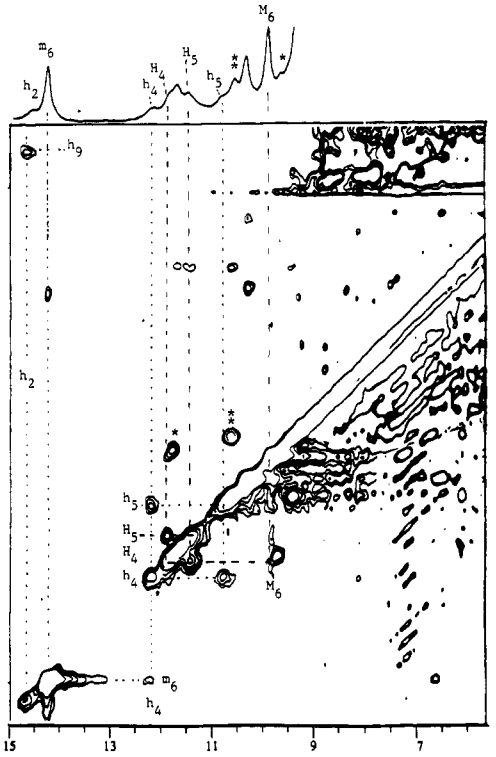

FIGURE 8: Low-field portion of the 500-MHz ^{1}H NMR NOESY spectrum (20-ms mixing time) of PHIX-HO-CN in ^2H_2O (pH 7.1) at 20 °C, illustrating dipolar contacts involving m_6 (8-CH_3) and h_2 of isomer Y and M_6 (5-CH_3) of isomer X. Other hyperfine-shifted residues in the 10–12 ppm window that exhibit NOESY (and MCOSY; not shown) cross peaks but cannot be assigned or attributed to isomers are labeled * and **.

likely geminal protons; the apparent line width (~120 Hz) for these partially resolved peaks precludes the detection of the expected weak COSY cross peak. The NOESY cross peaks from one proton from each pair to methyl peaks M_6 and m_6, the 5-CH_3 of the X isomer and the 8-CH_3 of the Y isomer (Figure 8), likely identify the adjacent propionate 6-α-CH_2 (H_4,H_5) and 7-α-CH_2 (h_4,h_5) pairs for the respective isomers. It is noted that neither the set M_6,H_5,H_4 nor the set m_6,h_5,h_4 exhibits NOESY cross peaks (or steady-state NOESY) to the upfield proton pairs H_{14},H_{17} or h_{14},h_{17}, respectively. The resolved low-field isomer X peak H_2 exhibits an intense NOESY cross peak to H_9, as shown in Figure 7F (approximately –40% steady-state NOE; not shown), which is indicative of a CH_2 group with no NOESY cross peak to any heme resonance. The most likely origin would be the β-CH_2 group for the coordinated His for isomer X, as observed in other related proteins (Thanabal et al., 1987; Lecomte & La Mar, 1986). A similar NOESY cross peak is observed between the partially resolved isomer Y peaks h_2 and h_9 (Figure 8), suggesting that H_2,H_9 and h_2,h_9 have similar structural origins in the two isomers. The other resonances in the 10–12 ppm window exhibit COSY, as well as intense NOESY, cross peaks (marked by * and ** in Figure 8B), but the absence of additional NOESY cross peaks precludes identification of the isomer origin or their assignment to substituents.

Labile Protons. The ^{1}H NMR spectra in ^1H_2O failed to exhibit significant intensity for signals from labile protons unless the spectrum was collected with a soft pulse sequence without excitation of the solvent line (not shown; see supplementary material). With the soft pulse trace, a total of nine labile proton signals with significant temperature dependence of their shifts (see supplementary material) were observed in the spectral window 12–16 ppm. Eight signals exhibit an intensity of one proton relative to M_1,m_i, and one exhibits with two-proton intensity. The apparent pairing of the peaks indicates five labile protons per isomer. Because of the severe spectral congestion and the rapid exchange with solvent (Cutnell et al., 1981), neither 1D nor 2D experiments yielded useful information on their assignments. However, it is concluded that at least one residue besides the expected proximal His places a labile proton close to the iron.

DISCUSSION

Substrate Binding. The presence of many fewer resonances in the cyanide complex of HO when a 2-fold-symmetric substrate (PHIII in Figure 3D or DHIII in Figure 5D) is compared to the native PHIX (Figure 3A) or its synthetic analog, DHIX (Figure 5A), argues for isomeric incorporation of the substrate in the binding pocket, with orientational disorder about the α,γ-meso axis. Similar heme orientational disorder is observed in the initial complex upon the assembly of apoprotein and heme and often at equilibrium for cytochrome b_5, Mb, and Hb (La Mar et al., 1981, 1983, 1985). The detailed isotopic labeling shows that the proposed heme disorder manifests itself differently in PHIX-HO-CN than in previously studied proteins, in that HO does not exhibit an interchange of the 3-CH_3 and 1-CH_3 hyperfine shifts (and vice versa) in the alternate isomers. The 1-CH_3 ↔ 3-CH_3 and 5-CH_3 ↔ 8-CH_3 interchange of environments had been considered diagnostic of heme orientational disorder. For the cyanide complex of substrate-bound HO, however, this interchange is not observed (i.e., 3-CH_3 environments for the two orientations are very similar), but can be traced to the unprecedented electronic structural properties of the heme (see below).

Much more direct evidence for heme orientational disorder about the α,γ-meso axis is obtained from the 2D NMR data in Figure 7. It is noted that in isomer X the 2-vinyl protons (H_2, H_{15}, and H_{16}) all exhibit strong dipolar contacts (Figure 7B) to protons with temperature-independent shifts in the 6–8 ppm window (H_7, and H_8), which is diagnostic of contact with an aromatic side chain. In contrast, the isomer X 3-CH_3 (M_1) fails to show such cross peaks (Figure 7H). However, it is the 3-CH_3 (m_1) of isomer Y that exhibits dipolar contacts to the aromatic side chain (h_7 and h_8), with very similar shifts to H_7, and H_8 of isomer X. Hence, the 3-CH_3 of isomer Y and the 2-vinyl group of isomer X experience essentially the same environment, providing direct evidence for heme orientational disorder about the α,γ-meso axis. The presence of a 1:1 ratio in the initially formed CN^- complex of PPIX-HO (Figure 3A), together with the multiplicity of peaks for high-spin PHIX-HO (Figure 2A), dictates that the heme orientational disorder is present in the uninhibited, functional form of the substrate-bound complex.

The present NMR studies provide little definitive information on the components of the substrate binding site. The low-field geminal protons H_2, H_9 for isomer X, together with the broad upfield single-proton peak x are consistent with the expectation of an axial His $C_\beta H_2$ and a ring CH, respectively (Emerson & La Mar, 1990a; Thanabal et al., 1987). Three partial residues have been identified: an aromatic side chain in contact with pyrrole B in isomer X (H_7,H_8) and pyrrole A in isomer Y, a $CHCH_3$ fragment (H_{11},M_{13}) in contact with the pyrrole A/B junction of isomer X, and a CH_2 fragment (H_{14},H_{17}) probably in contact with pyrrole D of isomer X and pyrrole C of isomer Y (h_{14},h_{17}). The number of hyperfine-shifted labile proton peaks strongly suggests a polar distal residue, quite possibly a His (Lecomte & La Mar, 1986; Thanabal et al., 1988). The fact that all labile protons

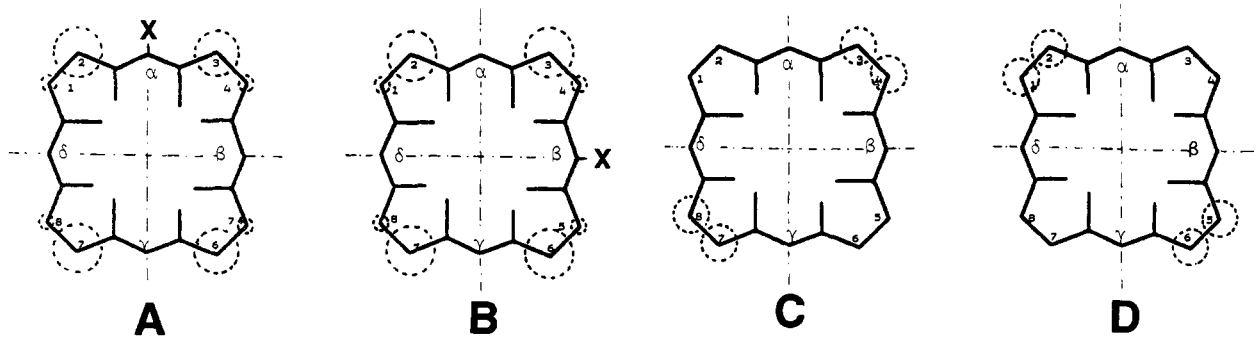

FIGURE 9: Patterns of the unpaired spin distribution about the hemin periphery in the highest bonding orbital resulting from raising (A) and lowering (B) the X carbon p_z orbital energy [as adapted from Walker and Simonis (1994)]. The size of the circle qualitatively indicates the population of the spin density and, hence, the contact shifts of the substituent. The unpaired spin distributions for hemin in various low-spin ferric myoglobins and hemoglobins are those shown in C and D.

exchange rapidly, some of which must arise from the proximal His as well as a distal residue, suggests that the active site in the substrate-bound complex is much more open and/or accessible to water than that of Mb or HRP (Cutnell et al., 1981; Thanabal et al., 1988). However, the presence of two isomers and the rapid exchange rates with solvent preclude more definitive identification of the labile proton peaks at this time. A less compact heme pocket in substrate-bound HO is also supported by the relatively few heme-amino acid dipolar contacts when compared to the same derivative of Mb or a heme peroxidase (Emerson & La Mar, 1990a; de Ropp et al., 1991).

It is noted that the pattern of hemin contact shifts, particularly for the 3-CH_3 and 2-vinyl of isomer X, is strongly perturbed by the protonation of the residue responsible for the pH influence depicted in Figure 4. In particular, the 3-CH_3 (M_1) and the 2-vinyl H_α (H_3) contact shifts for the X isomer increase and decrease strongly, respectively, at acidic pH. The 5-CH_3 peak (M_6) also moves upfield, thereby abolishing the unique spin density distribution observed above pH 7 (see below). It is unlikely that the titration involves the propionates, since the 3-CH_3 and 2-vinyl peaks are more strongly perturbed than the 5-CH_3 peaks (Figure 4), although the p*K* could well be for an amino acid side-chain carboxylate. What is more likely is that the titrating residue is linked to that residue responsible for the electronic influence described in the following section.

Hemin Electronic Structure

High-Spin Complex. The pattern of hyperfine shifts for PPIX-HO (Figure 2A) and DHIX-HO (Figure 2A) is similar to that of other ferric hemoproteins with axial His ligation (Satterlee, 1986). The low-field bias for the heme methyl envelope in the HO substrate complex more closely resembles that of HRP (Figure 2C) than that of met-Mb-H_2O (Figure 2D), indicating that the HO substrate complexes are not purely high-spin. This conclusion is in accord with recent resonance Raman studies that indicate a significant contribution from an intermediate spin state (Sun et al., 1993). The dominant contact shift pattern for primarily high-spin hemins is relatively insensitive to environment (Walker & Simonis, 1993); hence, detailed assignments were not pursued.

Low-Spin Cyanide Complex. The hyperfine shifts for the heme, as in all other characterized low-spin ferric systems (Walker & Simonis, 1993), are predominantly contact in origin and, hence, reflect the nature of the highest bonding porphyrin π orbital(s) interacting with the ferric ion. The dominant contact origin of the heme hyperfine shifts is directly supported by the large low-field 3-CH_3 and the strong low-field and upfield shifts for the 2-vinyl H_α and H_β's, respectively, of PHIX-HO-CN, as well as by the strongly upfield 2-H and 3-H shifts of DHIII-HO-CN (peaks H_{11} and H_{12} in Figure 5E). Hence, the peripheral substituent shifts directly reflect the distribution of π unpaired spin density about the heme periphery. Inspection of the data in Table 1 and Figures 3A and 5A reveals that the spin density in isomer X of PHIX-HO-CN is largest at positions 3 (methyl) and 2 (vinyl) and much smaller at positions 1 (CH_3) and 4 (vinyl), since neither of the latter two substituents exhibits contact shifts outside the 0–10 ppm window. Similarly, the 5- and 8-methyls of isomer X exhibit much smaller shifts than the 3-CH_3 or 2-vinyl, indicating minor spin density at those positions. On the other hand, the proposed assignment of 6-propionate H_α's (H_4 and H_5) well to the low-field of 5-CH_3 (M_6) dictates that the spin density is greater at position 6 than position 5. The failure to locate the 8-CH_3 of isomer X precludes detection of the relative spin densities at positions 7 and 8; however, the spin density is very small at the 8-CH_3 since the signal is not resolved from isomer X. Hence, the contact shift pattern observed for isomer X can be represented qualitatively by a spin density distribution about the porphyrin, as shown in Figure 9A.

A spin density distribution such as that shown in Figure 9A, which emphasizes asymmetry within a pyrrole rather than between adjacent pyrroles, is unprecedented in the electronic structure of any low-spin ferric hemoprotein characterized to date (Satterlee, 1986) or any model compound of a native hemin derivative (Walker & Simonis, 1993). The contact shift pattern in previously studied low-spin ferric hemoproteins is dominated by the selective spin delocalization from the iron into one or the other of the two essentially degenerate components of the porphyrin $3e_\pi$ orbitals shown schematically in Figure 9C,D. The selectivity in the delocalization is due to the raising of the iron d_{xz}, d_{yz} orbital degeneracy by the protein rhombic field (Shulman et al., 1971), which has been shown to result from the orientation of the axial His in Mb (Emerson & La Mar, 1990b). The heme contact shift pattern in these proteins is characterized by large contact shifts for all substituents on pairs of trans pyrroles, i.e., pyrroles A and B (Figure 9C) or pyrroles C and D (Figure 9D). An orientation of the axial His imidazole along meso positions leads to comparable spin density at all four pyrroles and at both positions on a given pyrrole (Peyton et al., 1989) and, hence, does not account for the presently observed contact shift pattern. A mechanism where primarily the d orbital energies are perturbed by the protein matrix (Shulman et al., 1971) does not account for the present spin distribution in PPIX-HO-CN. Indeed, it is necessary to propose that the HO protein

matrix directly perturbs the molecular orbitals of the hemin substrate.

The only precedent for a π spin distribution in a low-spin ferric hemin with properties similar to those described here lies in recent NMR work on model hemes selectively *electronically* perturbed at a meso position (Tan et al., 1994). Thus, if the synthetic 4-fold-symmetric tetraphenylporphyrin low-spin iron(III) complex is subject to enhanced electron-donating or electron-withdrawing substitution at one meso phenyl group (labeled X in Figure 9A) relative to the other three, the π spin density distribution within a given pyrrole becomes highly asymmetric, with resulting patterns of contact shifts or spin density distributions as shown in Figure 9A,B, respectively. The observed contact shift pattern, moreover, could simply be modeled by Hückel calculations when the energy of the substituted meso carbon p_z orbital was lowered or raised by electron-donating or -withdrawing substituents, respectively. Hence, the hemin contact shift pattern in the cyanide complex of substrate-bound HO is consistent with that resulting from a protein *residue selectively interacting with the heme near the α-meso (and/or γ-meso) position so as to donate electron density* or a residue interacting selectively with the β-meso (and/or δ-meso) position that withdraws electron density. A carboxylate side chain of an Asp or a Glu over the α-meso carbon could be responsible for this effect, and its protonation at low pH would rationalize the pH influence that abolishes the unusual electronic structure for the heme at low pH.

Some of the strongest dipolar contacts observed to this heme are due to the residue that gives rise to the $CHCH_3$ (peaks H_{11} and M_{13} in Figures 3A and 7C), which interacts with the 3-CH_3, α-meso-H, and 2-vinyl substituents, i.e., precisely at the junction of pyrroles A and B. The identity of the residue could not be established further, but the observed fragment is consistent with Val, Ile, Leu, and Thr. The strongest NOE from the 3-CH_3 is to an apparent peak M_{12}, which cannot be assigned at this time. A side-chain carboxylate near the α-meso bridge is not detectable by NMR at this time. Clearly, many more assignments are needed to locate and identify the heme contacts of interest. Such studies may become practical when sufficient amounts of symmetric hemin become available.

It is noted that the contact shift pattern in DHIX-HO-CN is similar to that in PHIX-HO-CN, in that the largest π spin density gives rise to the large upfield 2-H and 3-H contact shifts, as shown in Figure 5E. Hence, the peculiar π-spin distribution noted above (i.e., Figure 9A) is qualitatively characteristic of all cyanide complexes of substrate-bound HO. However, as is clearly shown for PPIX-HO-CN, there are significant quantitative differences in the contact shift pattern for the two orientations of the protohemin IX. The 3-CH_3 shift (and, hence, spin density) of isomer Y (m_1) is significantly larger than that of isomer X (M_1), and since a 2-vinyl signal is not observed in the upfield window for isomer Y, the π contact shift (and, hence, spin density) at the 2-position is smaller in isomer Y than in isomer X. Thus, the Y isomer exhibits the asymmetry characteristic of the orbital in Figure 9A much less than does isomer X. In fact, the larger shift for the 8-CH_3 (m_6) in Y than for the 5-CH_3 (M_6) in the X isomer indicates that the spin distribution for isomer Y is somewhere between that in Figure 9A and the more conventional pattern observed in cytochromes, Mb, or Hb, i.e., that in Figure 9C, where the large shifts are from *trans* pyrroles (3-CH_3, 8-CH_3). Thus, the protein influence on the porphyrin orbitals appears to differentiate between the heme orientations in the substrate binding site.

Steric Influences on Bound Cyanide. In contrast to the large hyperfine shifts for the heme and axial His which are dominated by contact shifts (Walker & Simonis, 1993), those for non-coordinated residues arise wholly from the dipolar interaction, whose shifts are given by

$$\delta_{dip} = (\Delta\chi_{ax}F_{ax} + \Delta\chi_{rh}F_{rh})\mathbf{R}(\alpha,\beta,\gamma) \quad (1)$$

where $\Delta\chi_{ax}$ and $\Delta\chi_{rh}$ are the axial and rhombic magnetic anisotropies, respectively, F_{ax} and F_{rh} are geometric factors that locate a given proton in the heme-centered pseudosymmetry coordinate system, respectively, and $\mathbf{R}(\alpha,\beta,\gamma)$ is a rotation matrix that relates the magnetic axes to the heme pseudosymmetry coordinate system (Emerson & La Mar, 1990b; Rajarathnam et al., 1992, 1993; Qin et al., 1993). For a given magnetic anisotropy, changes in shifts for a given functional group must reflect a change in the orientation of the group relative to the heme (*i.e.*, change in F_{ax} and F_{rh}), a change in the orientation of the magnetic anisotropy tensor (change in $\mathbf{R}(\alpha,\beta,\gamma)$), or possibly both. At 20 K the cyanide complex of substrate-bound HO exhibited a low quality ESR spectrum, with the low low-field $g_z \sim 3.5$ (not shown) close to the values obtained from the same Mb complex (Hori, 1971). Hence, it appears that the magnetic anisotropy is very similar in both heme orientations of HO and in Mb.

In low-spin ferric myoglobin, hemoglobin, and cytochrome b_5, it has been observed that the non-coordinated amino acid protons exhibit very similar, if not identical, δ_{dip} values for the two alternate heme orientations (Lecomte et al., 1985; Peyton et al., 1989; Lee et al., 1993; Guiles et al., 1993), showing that neither the disposition of non-coordinated residues nor the orientation of the magnetic axes is significantly different for the two heme orientations. When distal residues in myoglobin are mutated, conserved residues experience substantial and systematic shift changes that have been demonstrated quantitatively to arise solely from a reorientation of the major magnetic axis (Rajarathnam et al., 1992, 1993; Qin et al., 1993). Moreover, it was possible to establish that the orientation of the major magnetic axis is determined by the Fe–C–N tilt or that the orientation of the major magnetic axis reflects the orientation of the Fe–CN vector (Emerson & La Mar, 1990b; Rajarathnam et al., 1992).

For PPIX-HO-CN, two sets of resonances have been attributed to strongly dipolar shifted non-coordinated residues: the CH_2 group represented by H_{14},H_{17} (X isomer) and h_{14},h_{17} (Y isomer) and the $CHCH_3$ fragment (H_{10}, M_{13}) observed upfield only for isomer X. The δ_{dip} values for H_{14},H_{17} and h_{14},h_{17} differ significantly, and for the $CHCH_3$ in isomer Y, the methyl must have at least a 3 ppm smaller δ_{dip}. The major magnetic axis, and hence the orientation of the Fe–CN vector, likely differs significantly between the X and Y isomers. Recent work with cyanometmyoglobin (Rajarathnam et al., 1992) and the cyanide complex of horseradish peroxidase (G. N. La Mar, Z. Chen, G. Hernández, and J. S. de Ropp, manuscript in preparation) has shown that high-field dipolar-shifted resonances generally result only if the major magnetic axis is tilted from the heme normal. Thus, it appears that the heme orientation in PPIX-HO-CN significantly influences the magnitude and/or direction of tilt of the FeCN unit.

CONCLUSIONS

We have recently proposed two alternatives for reaction of the porphyrin ring with the intact iron–dioxygen complex, leading to α-*meso*-hydroxyheme (Wilks & Ortiz de Montellano, 1993): (a) nucleophilic addition of the terminal oxygen

of the unprotonated complex [FeOO] to the α-meso carbon to give a peroxo-bridged intermediate [FeO–OC-*meso*]; (b) electrophilic addition of the terminal oxygen of the protonated complex [FeOOH] to the porphyrin ring with concomitant cleavage of the dioxygen bond. These two mechanisms are consistent with the observations that H_2O_2, but not alkyl peroxides, replaces cytochrome P-450 reductase and NADPH in heme hydroxylation, that a ferryl species is not involved in the heme degradation pathway, and that the protein catalyzes highly regiospecific cleavage of the heme ring. The electronic structure, as reflected in the contact shift pattern, of isomer X of PPIX-HO-CN reflects a protein-induced perturbation that appears to stabilize (donate electron density to) the p_z orbital of the α-meso carbon, possibly by strong interaction with an as yet unidentified residue. This interaction, moreover, appears to be modulated by solution pH. Such an interaction would facilitate nucleophilic rather than electrophilic attack at the α-meso position.

Resonance Raman studies (Sun et al., 1993) have shown that the heme is axially coordinated to a histidine that appears to be neither ionized nor strongly hydrogen-bonded. The resulting decreased ability of the imidazole to donate electrons to the iron makes dioxygen bond cleavage more difficult and may channel the reaction to biliverdin formation rather than to formation of a ferryl species. The weak participation of the histidine ligand also suggests that residues in the distal side of the heme pocket may facilitate addition of the intact iron-coordinated oxygen molecule to the meso carbon of the porphyrin. The present NMR results indeed show that the protein environment exerts a direct influence on the hemin electronic structure that facilitates the selective cleavage of the α-meso position. Moreover, it appears as if distal steric influences also contribute to the appropriate orientation of a coordinated oxygen molecule. The pattern of dipolar-shifted signals for non-coordinated residues suggests that the distal pocket exerts steric influence to orient the ligand. The fact that the residues show upfield dipolar shifts if the FeCN unit is tilted toward or away from the shifted residue (Rajarathnam et al., 1992) suggests that the FeOO unit is oriented either toward or away from the α-meso position in isomer X; the former orientation would clearly facilitate the transfer of the terminal oxygen donor to the α-meso carbon.

The isomeric incorporation of protohemin IX into the substrate pocket of HO clearly is relevant to its function. We conclude above that the protein appears to exert both an electronic influence on the substrate and a steric effect on the bound ligand that facilitates stereospecific cleavage of the α-meso position. The selectivity of the reaction is unaffected by this isomerism, since the α,γ-meso axis is conserved. However, both influences differ for the two isomers, and it is therefore possible that the rate of reaction, if not the stereospecificity, differs for the two orientations of PPIX. Since the pattern of the hyperfine shifts for the two orientations of the cyano complex of deuterohemin IX differs from that of either orientation for protohemin IX, the large variations in activity for different synthetic hemins (Frydman & Frydman, 1987) may be related to the degree of electronic and steric activation exerted by the protein matrix. It is expected that the residues of the heme pocket can be further elucidated by solution solvent ^1H NMR, but such studies need to be carried out on an HO complex with a homogeneously bound substrate, i.e., a symmetric hemin. The preparation of significant amounts of several examples of such hemins is underway, as are studies directed toward detecting biphasic reaction kinetics and pH influences thereon.

ACKNOWLEDGMENT

The authors are indebted to Drs. J. S. de Ropp and Z. Chen for experimental assistance.

SUPPLEMENTARY MATERIAL AVAILABLE

Two figures containing ^1H NMR spectra of PHIX-HO-CN in ^1H_2O and the effect of pH on ^1H NMR spectra in PPIX-HO-CN in ^2H_2O (2 pages). Information for obtaining this material can be found on the masthead page.

REFERENCES

Bax, A. (1982) *Two dimensional nuclear magnetic resonance in liquids*, D. Reidel Publishing Co., Dordrecht, The Netherlands.
Beale, S. I. (1993) *Chem. Rev. 93*, 785–802.
Bonkovsky, H. L., Healey, J. F., & Pohl, J. (1990) *Eur. J. Biochem. 189*, 155–166.
Cutnell, J. D., La Mar, G. N., & Kong, S. B. (1981) *J. Am. Chem. Soc. 103*, 3567–3572.
de Ropp, J. S., Yu, L. P., & La Mar, G. N. (1991) *J. Biomol. Nucl. Magn. Reson. 1*, 175–190.
Emerson, S. D., & La Mar, G. N. (1990a) *Biochemistry 29*, 1545–1555.
Emerson, S. D., & La Mar, G. N. (1990b) *Biochemistry 29*, 1556–1566.
Evans, C.-O., Healey, J. F., Greene, Y., & Bonkovsky, H. L. (1991) *Biochem. J. 273*, 659–666.
Frydman, R. B., & Frydman, B. (1987) *Acc. Chem. Res. 20*, 250–256.
Fuhrhop, J.-H., & Smith, K. M. (1975) in *Porphyrins & Metalloporphyrins* (Smith, K. M., Ed.) pp 773–774, Elsevier, Amsterdam.
Guiles, R. D., Basus, V. J., Sarma, S., Malpure, S., Fox, K. M., Kuntz, I. D., & Waskell, L. (1993) *Biochemistry 32*, 8329–8340.
Hore, P. J. (1983) *J. Magn. Reson. 54*, 539–542.
Hori, H. (1971) *Biochim. Biophys. Acta 251*, 227–235.
Ishikawa, K., Sato, M., Ito, M., & Yoshida, T. (1992) *Biochem. Biophys. Res. Commun. 182*, 981–986.
La Mar, G. N., Burns, P. D., Jackson, J. T., Smith, K. M., Langry, K. C., & Strittmatter, P. (1981) *J. Biol. Chem. 256*, 6075–6079.
La Mar, G. N., Davis, N. L., Parish, D. W., & Smith, K. M. (1983) *J. Mol. Biol. 168*, 887–896.
La Mar, G. N., Yamamoto, Y., Jue, T., Smith, K. M., & Pandey, R. K. (1985) *Biochemistry 24*, 3826–3831.
La Mar, G. N., & de Ropp, J. S. (1993) in *Biological Magnetic Resonance* (Berliner, L. J., & Reuben, J., Eds.) Vol. 17, pp 1–78, Plenum Press, New York.
Lecomte, J. T. J., & La Mar, G. N. (1986) *Eur. Biophys. J. 13*, 373–381.
Lecomte, J. T. J., Johnson, R. D., & La Mar, G. N. (1985) *Biochim. Biophys. Acta 829*, 268–274.
Lee, K.-B., La Mar, G. N., Mansfield, K. E., Smith, K. M., Pochapsky, T. C., & Sligar, S. G. (1993) *Biochim. Biophys. Acta 1202*, 189–199.
Maines, M. D. (1992) *Heme Oxygenase—Clinical Applications and Functions*, CRC Press, Boca Raton, FL.
Maines, M. D., Trakshel, G. M., & Kutty, R. K. (1986) *J. Biol. Chem. 261*, 411–419.
Marion, D., & Wüthrich, K. (1983) *Biochem. Biophys. Res. Commun. 113*, 967–974.
McCoubrey, W. K., Jr., & Maines, M. D. (1993) *Arch. Biochem. Biophys. 302*, 402–408.
Peyton, D. H., La Mar, G. N., & Gersonde, K. (1988) *Biochim. Biophys. Acta 954*, 82–94.
Peyton, D. H., La Mar, G. N., Pande, U., Ascoli, F., Smith, K. M., Pandey, R. K., Parish, D. W., Bolognesi, M., & Brunori, M. (1989) *Biochemistry 28*, 4880–4887.

Qin, J., La Mar, G. N., Ascoli, F., & Brunori, M. (1993) *J. Mol. Biol. 231*, 1009–1023.
Rajarathnam, K., La Mar, G. N., Chiu, M. L., & Sligar, S. G. (1992) *J. Am. Chem. Soc. 114*, 9048–9058.
Rajarathnam, K., Qin, J., La Mar, G. N., Chiu, M. L., & Sligar, S. G. (1993) *Biochemistry 32*, 5670–5680.
Satterlee, J. D. (1986) *Annu. Rep. Nucl. Magn. Reson. Spectrosc. 17*, 79–178.
Sette, M., de Ropp, J. S., Hernández, G., & La Mar, G. N. (1993) *J. Am. Chem. Soc. 115*, 5237–5245.
Shibahara, S., Muller, R., Taguchi, & Yoshida, T. (1985) *Proc. Natl. Acad. Sci. U.S.A. 82*, 7865–7869.
Shulman, R. G., Glarum, S. H., & Karplus, M. (1971) *J. Mol. Biol. 57*, 93–115.
Smith, K. M., Fujinari, E. M., Langry, K. C., Parish, D. W., & Tabba, H. D. (1983) *J. Am. Chem. Soc. 105*, 6638–6646.
Smith, K. M., Parish, D. W., & Inouye, W. S. (1986a) *J. Org. Chem. 51*, 666–671.
Smith, K. M., Miura, M., & Morris, I. K. (1986b) *J. Org. Chem. 51*, 4660–4667.
Smith, K. M., Leung, H. K., & Parish, D. W. (1988) *J. Chem. Res., Miniprint* 2743–2762.
Stevens, C. F., & Wang, Y. (1993) *Nature 364*, 147–1481.
Sun, J., Wilks, A., Ortiz de Montellano, P. R., & Loehr, T. M. (1993) *Biochemistry 32*, 14151–14157.
Takahashi, S., Wang, J., Rousseau, D. L., Ishikawa, K., Yoshida, T., Host, J. R., & Ikeda-Saito, M. (1994) *J. Biol. Chem. 269*, 1010–1014.
Tan, H., Simonis, U., Shokhirev, No., & Walker, F. A. (1993) *J. Am. Chem. Soc.* (submitted for publication).
Tenhunen, R., Marver, H. S., & Schmid, R. (1969) *J. Biol. Chem. 244*, 6388–6394.
Thanabal, V., de Ropp, J. S., & La Mar, G. N. (1987) *J. Am. Chem. Soc. 109*, 7516–7525.
Thanabal, V., de Ropp, J. S., & La Mar, G. N. (1988) *J. Am. Chem. Soc. 110*, 3027–3035.
Verma, A., Hirsch, D. J., Glatt, C. E., Ronnett, G. V., & Snyder, S. H. (1993) *Science 259*, 381–384.
Walker, F. A., & Simonis, U. (1994) in *Biological Magnetic Resonance* (Berliner, L. J., & Reuben, J., Eds.) Vol. 12, pp 133–274, Plenum Press, New York.
Wilks, A., & Ortiz de Montellano, P. R. (1993a) *J. Biol. Chem. 268*, 22357–22363.
Wilks, A., & Ortiz de Montellano, P. R. (1993b) *J. Inorg. Biochem. 51*, 269.
Yoshida, T., & Kikuchi, G. (1978) *J. Biol. Chem. 253*, 4224–4229.
Yoshida, T., & Kikuchi, G. (1979) *J. Biol. Chem. 254*, 4487–4491.
Yoshida, T., Biro, P., Cohen, T., Muller, R., & Shibahara, S. (1988) *Eur. J. Biochem. 171*, 457–461.
Yoshinaga, T., Sassa., S & Kappas, A. (1982) J. Biol. Chem. 257, 7778–7785.
Zhuo, M., Small, S. A., Kandel, E. R., & Hawkins, R. D. (1993) *Science 260*, 1946–1950.